optica

Dispersive soft x-ray absorption fine-structure spectroscopy in graphite with an attosecond pulse

Bárbara Buades,[1] Dooshaye Moonshiram,[2] Themistoklis P. H. Sidiropoulos,[1] [iD] Iker León,[1] Peter Schmidt,[1] Irina Pi,[1] Nicola Di Palo,[1] Seth L. Cousin,[1] Antonio Picón,[1,3] Frank Koppens,[1,4] and Jens Biegert[1,4,*] [iD]

[1]ICFO-Institut de Ciencies Fotoniques, The Barcelona Institute of Science and Technology, 08860 Castelldefels, Barcelona, Spain
[2]Max Planck Institute for Chemical Energy Conversion, Stiftstr. 34-36, D-45470 Mülheim an der Ruhr, Germany
[3]Grupo de Investigación en Aplicaciones del Láser y Fotónica, Departamento de Física Aplicada, University of Salamanca, E-37008 Salamanca, Spain
[4]ICREA, Pg. Lluis Companys 23, 08010 Barcelona, Spain
*Corresponding author: jens.biegert@icfo.eu

Phase transitions of solids and structural transformations of molecules are canonical examples of important photo-induced processes whose underlying mechanisms largely elude our comprehension due to our inability to correlate electronic excitation with atomic position in real time. Here, we present a decisive step towards such new methodology based on water-window covering (284–543 eV) attosecond soft x-ray pulses that can simultaneously access electronic and lattice parameters via dispersive x-ray absorption fine-structure (XAFS) spectroscopy. We validate this approach with an identification of the σ^* and π^* orbital contributions to the density of states in graphite simultaneously with its lattice's four characteristic bonding distances. This work demonstrates the potential of dispersive XAFS, in combination with attosecond pulses, as a powerful investigative tool that is equally applicable to gas, liquid, and condensed phase.   © 2018 Optical Society of America under the terms of the OSA Open Access Publishing Agreement

OCIS codes: (320.0320) Ultrafast optics; (320.7110) Ultrafast nonlinear optics; (260.6048) Soft x-rays; (300.6560) Spectroscopy, x-ray; (300.1030) Absorption.

https://doi.org/10.1364/OPTICA.5.000502

1. INTRODUCTION

X-ray absorption fine-structure (XAFS) spectroscopy is a powerful element-specific technique providing electronic as well as structural and chemical information with atomic resolution [1–4]. In XAFS, electronic information is extracted from the near-edge XAFS (XANES or NEXAFS), which arises from transitions from inner-shell orbitals to unoccupied electronic states near the Fermi energy level. Its measurement requires high spectral resolution to resolve its features, which occur within only a few electron volts. Structural information is mainly obtained from the extended XAFS (EXAFS), which extends over several hundred electron volts above the absorption edge, and it arises from the scattering of photo-emitted core electrons on neighboring atoms. While XANES and EXAFS are both well-established methods, and quick-scan or dispersive setups permit a relatively rapid acquisition of EXAFS [5,6], crucially lacking so far has been the capacity to connect electronic with structural information in real time, i.e., faster than the typical tens of femtoseconds dephasing time of electronic wave packets [7]. The capability to probe the connection between a material's electronic excitation and lattice reordering provides a new powerful tool to gain insight into the real-time

evolution on nonequilibrium dynamics such as, e.g., structural and electronic phase transitions.

Here, we achieve this key requirement through the simultaneous measurement of XANES and EXAFS with an isolated attosecond soft x-ray (SXR) pulse. Until now, the limiting factor for such implementation was the combined requirement for broadband spectral coverage beyond an absorption edge and the ultrashort temporal duration of the x-ray pulses. Thus, with the advent of high-harmonic generation (HHG) light sources [8], a novel tabletop tool has emerged that was successfully applied to XANES in solids [9–14] and for molecules [15,16]. However, it has only been recently that all requirements for the desired combined XANES and EXAFS were met by the generation of isolated attosecond SXR pulses with coverage of the entire water window (284–534 eV) [17–19]. These pulses provide the ultrafast temporal resolution in combination with sufficient spectral coverage in a photon energy range that accesses core-level transitions, thus offering element specificity.

2. XAFS IN GRAPHITE

We demonstrate the concept of XAFS in graphite with an isolated attosecond water-window SXR pulse that enables the

Fig. 1. XAFS–Simultaneous XANES and EXAFS with an isolated attosecond SXR pulse. (a) Shown is the spectrum of the isolated attosecond pulse spanning the entire SXR water window (284–543 eV) at once. Overlaid as vertical lines are the positions of accessible K- (orange), L- (green), and M-shell (blue) absorption edges. Note that the depletion at the C-edge is due to the ubiquitous hydrocarbon contamination originating from turbo pumps in the beamline. (b) shows the XAFS measurement in graphite in which the XANES is highlighted in red and the EXAFS in blue. The shading around the absorbance indicates the confidence band of the measurement. (c) indicates that spectral components with photon energy above 284 eV access 1s carbon K-shell core-level electrons. Transitions to bound states close to the Fermi edge are known as XANES, and transition into the continuum, giving rise to the EXAFS. XANES provides orbital sensitivity depending on the angle of the impinging x-ray pulse field vector relative to the basal plane normal of the sample, while EXAFS predominantly provides local structural information as it is related to the scattered electron wave from the absorber atom on the neighboring atoms. Note that no hard boundary exists between XANES and EXAFS, and that the color separation is solely chosen to indicate the predominant contribution to the measurement.

Fig. 2. XAFS identifies different electronic orbitals. (a) shows the XANES region for three measurements in which the angle of incidence of the impinging attosecond SXR pulse is varied with respect to the basal plane normal of the sample. Normal incidence [shown also in (b) and (c)] probes states in the basal plane, while any deviation from normal incidence also probes components out of the basal plane. (b) and (c) show results from DFT calculations using BAND [22–24]. The DOSs correspond to the lowest unoccupied states π^* (b) and σ^* (c) in the conduction band. Two main features can be identified from (a) at 285.5 eV and 292.5 eV, corresponding to $1s \rightarrow \pi^*$ and $1s \rightarrow \sigma^*$ transitions, respectively.

simultaneous acquisition of carbon K-edge XANES and EXAFS, thus providing combined electronic and structural information. The spectrum supporting a sub-300-as-duration pulse [18] is shown in Fig. 1(a). This spectrum covers a region 50 eV below the carbon K-edge (284 eV) up to the oxygen K-edge (543 eV), thus including the K-edge of nitrogen (410 eV) as well as many L and M edges that are relevant to biology and material science. The linearly polarized attosecond pulse was generated via HHG and provided adequate photon flux of 7.3×10^7 photons/s at 1-kHz repetition rate for the 320-eV bandwidth; details regarding the source can be found in [19]. The attosecond SXR pulse was focused with an elliptical mirror (Zeiss) onto a 95-nm-thin graphite sample that was mounted on a 50-nm Si_3N_4 substrate. The transmitted signal was analyzed by a home-built SXR spectrograph, which consisted of a flat-field imaging grating (Hitachi, 2400 lines/mm) and a Peltier-cooled, back-illuminated charge-coupled device (CCD) camera (PIXIS-XO-2048B, Princeton Instruments). To maximize photon flux on the CCD, the sample plane coincided with the entrance slit plane of the spectrograph; thus, without any entrance slit, the SXR focal spot determined the spectrograph's resolution to 1/1000, i.e., 0.3 eV at 300 eV. This spectral resolution is sufficient to resolve fine structure peaks of electronic orbitals and could be improved even further with a new spectrometer design to access, e.g., vibronic states. Figure 1(b) shows the measured absorbance from dispersive XAFS, which

is determined according to $-\log[S/S_0]$, where S is the spectral intensity through the sample, and S_0 the reference signal measured through only the 50-nm Si_3N_4 membrane. Clearly visible in the XAFS are sharp absorption features in the XANES region of the spectrum [Fig. 1(b), red curve] and oscillations in the EXAFS region [Fig. 1(b), blue curve].

Graphite consists of equally oriented graphene layers that interact via Van der Waals forces. In each graphene layer, the carbon atoms form strong covalent bonds and are orientated in a hexagonal lattice with four carbon atoms per unit cell. Each carbon atom has six electrons, of which two are located at the 1s core shell, and the other four electrons occupy the valence shells ($2s^2, 2p^2$). Three valence shell electrons form covalent bonds in graphite through an sp^2 hybridization. The fourth valence electron has p symmetry with an orientation perpendicular to the graphene plane (p_z hereafter) and binds via Van der Waals forces to the neighboring layers. The sp^2 orbitals form σ states in the sheet plane, and p_z forms a π state, which is the highest occupied state [20,21]. The antibonding states, σ^* and π^*, are unoccupied in graphite and form the conduction band. The different symmetries of the two antibonding states, σ^* and π^*, become apparent when comparing the density of states (DOSs) of the two different bands. Figures 2(b) and 2(c) show the corresponding orbitals calculated with the density functional theory (DFT) code BAND [22–24]; see Supplement 1 for further information.

A. Electronic Structure–XANES

XANES at the carbon K-shell edge results from dipole-allowed transitions from the 1s state to the lowest unoccupied states,

σ^* and π^*. Figure 2(a) shows the XANES part of the normalized XAFS spectrum taken at different incident angles of the linearly polarized attosecond SXR pulses with respect to the graphite basal plane normal. What we found, independent of the incident angle, is a clear rising edge at (292.6 ± 0.3) eV, which is followed by undulations of the absorption spectrum. From symmetry considerations, it is apparent that the edge arises due to the $1s \rightarrow \sigma^*$ transition, indicated in Fig. 2(c). Varying the incidence angle from 0 to 20 deg, a second peak appears at (285.5 ± 0.3) eV with an amplitude that increases as the incident angle is further increased to 35 deg. The clear field polarization dependence of the peak at 285.5 eV allows us to identify this as $1s \rightarrow \pi^*$ transition, since the π^* is formed by p_z, which is orientated perpendicular to the sample plane. At normal incidence, graphite's plane is perpendicular to the beam propagation direction; thus, the attosecond pulse's linearly polarized electric field probed only in-plane states, σ^*, consisting of sp^2. By tilting the sample, hence changing the angle of incidence from 0 to 35 deg, an electric field component along p_z is induced, which excites the $1s \rightarrow \pi^*$ transition. We find that these features, measured with the attosecond source, are in excellent agreement with predicted values as well as with electronic transitions [25–32] measured at synchrotron light sources. We note that the identified features are different from optical absorption measurements in which the $\pi \rightarrow \pi^*$ transition is only excited for in-plane polarization [20]; thus the difference with an x-ray measurement arises from the different initial states leading to different symmetry-allowed final states. The measurement accuracy is also sufficient to identify the weak feature, between the π^* and σ^* resonances at about 289 eV, as an interlayer state arising from small residual material impurities [32].

B. Lattice Structure–EXAFS

We turn to analyzing the EXAFS region to retrieve information about graphite's lattice conformation. We recall that EXAFS arises from the interference of excited photoelectrons with backscattered photoelectrons off neighboring lattice atoms, leading to constructive and destructive interference of the absorbing atom's electronic density and thus to oscillations in the measured extended absorption spectrum. The blue part of the measured absorption curve, shown in Fig. 1(b), displays the EXAFS of graphite. We deduce the bond length from these oscillations with the aid of the Athena and Artemis software packages [33] and perform multiple scattering path simulations with FEFF [34]; details are found in Supplement 1. In short, after background correction and conversion into wavenumber space, shown in Fig. 3(b), curve fitting is performed based on the EXAFS equation with scattering phases and amplitudes from FEFF [34]. Figure 3(c) shows the transformed amplitudes in which we identify three prominent peaks corresponding to the scattering contributions from the first, second, third, and fourth neighboring carbon atoms. Note that while only the amplitudes of the Fourier transform to R-space are shown in Fig. 3(c), our fit takes the phase shifts also into account, thereby resulting in a fitting accuracy of better than 2%. From our fit, we identify the first apparent peak at 1.35 Å, which, in accordance with [35,36], arises due to the scattering with the nearest neighbor at around 1.42–1.44 Å. The second peak represents the summed contribution of the second and third neighbor atoms at 2.47 Å and 2.87 Å with coordination numbers 6 and 3, respectively;
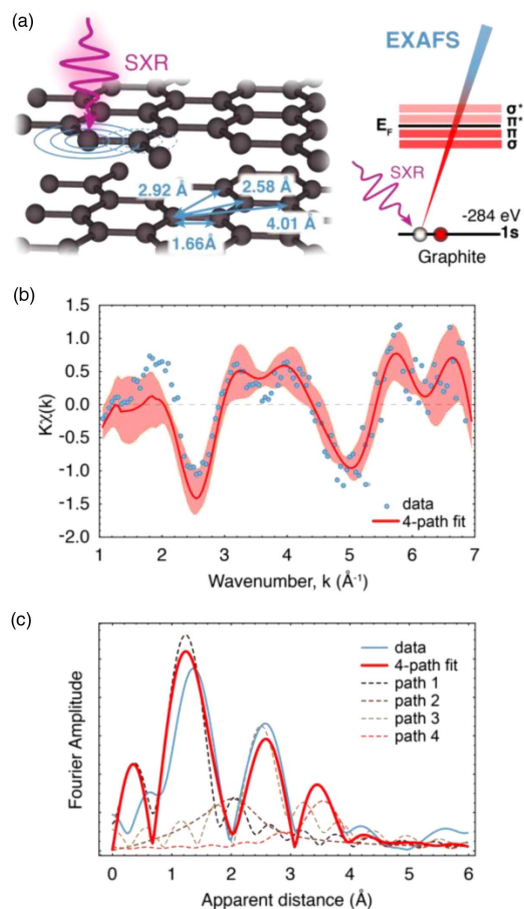
Fig. 3. Bond distances from EXAFS. (a) shows two layers of graphite together with the identified bond distances. The experimental EXAFS is shown by the blue circles in (b) together with the back-transformed fit (solid red line) and the fit's uncertainty (red shaded area). (c) shows the Fourier amplitude of the experimental data together with the individual contributions from the first four scattering paths (dashed lines). The summed scattering contribution is shown by the solid red line and, considering the scattering phases, results in a 2% fit accuracy. Note that the experimental spectra correspond to k values of 1.18 to 6.90 Å^{-1}.

see Supplement 1. Lastly, the third peak represents the scattering from the fourth nearest carbon atom at around 3.77 Å.

Finally, the analysis of the overall spectrum yields bond distances of (1.66 ± 0.03) Å, (2.58 ± 0.12) Å, (2.92 ± 0.03) Å, and (4.01 ± 0.10) Å. These bond distances from XAFS are identified in Fig. 3(a) and are in excellent agreement with DFT calculations and carbon K-edge EXAFS measurements conducted at synchrotron sources [35].

3. CONCLUSIONS

In conclusion, we demonstrate that XAFS with an attosecond SXR pulse presents a powerful new tabletop methodology to simultaneously probe electronic states and atomic positions in condensed phase. We validate dispersive XAFS with an attosecond pulse through a simultaneous identification of the σ^* and π^* orbitals in graphite in synchronicity with the material's four characteristic bonding distances. Further, the change of angle of incidence of the attosecond pulse permits distinguishing the various orbital contributions to the DOS of the material.

This capability offers the potential to perform x-ray spectroscopy with attosecond resolution, giving rise to a completely new technique to explore *in situ* electron-phonon interactions and to image how multibody correlations arise during a material's phase transition or the formation of the superconducting state. This work thus provides a powerful real-time investigative tool to access the characteristic time scale of electronic motion to resolve charge migration, electron-electron correlation, electron-nuclear scattering, and structural transitions. Finally, the access to core-level states in synchronicity with valence and conduction band states will enable the investigation of core, valence, and lattice correlations on a previously unprecedented attosecond time scale.

See Supplement 1 for supporting content.

REFERENCES

1. D. E. Sayers, E. A. Stern, and F. W. Lytle, "New technique for investigating noncrystalline structures: Fourier analysis of the extended x-ray—absorption fine structure," Phys. Rev. Lett. **27**, 1204–1207 (1971).
2. G. Hähner, "Near edge X-ray absorption fine structure spectroscopy as a tool to probe electronic and structural properties of thin organic films and liquids," Chem. Soc. Rev. **35**, 1244–1255 (2006).
3. K. Sauer, J. Yano, and V. K. Yachandra, "X-ray spectroscopy of the photosynthetic oxygen-evolving complex," Coord. Chem. Rev. **252**, 318–335 (2008).
4. H. Ade and H. Stoll, "Near-edge X-ray absorption fine-structure microscopy of organic and magnetic materials," Nat. Mater. **8**, 281–290 (2009).
5. R. Frahm, "Quick scanning EXAFS: first experiments," Nucl. Instrum. Methods Phys. Res. Sect. A **270**, 578–581 (1988).
6. B. R. Dobson, "Quick scanning EXAFS facilities at Daresbury SRS," Synchrotron Radiat. News **7**(1), 21–24 (1994).
7. M. Vacher, L. Steinberg, A. J. Jenkins, M. J. Bearpark, and M. A. Robb, "Electron dynamics following photoionization: decoherence due to the nuclear-wave-packet width," Phys. Rev. A **92**, 040502 (2015).
8. F. Krausz and M. Ivanov, "Attosecond physics," Rev. Mod. Phys. **81**, 163–234 (2009).
9. S. L. Cousin, F. Silva, S. Teichmann, M. Hemmer, B. Buades, and J. Biegert, "High-flux table-top soft x-ray source driven by sub-2-cycle, CEP stable, 185-μm 1-kHz pulses for carbon K-edge spectroscopy," Opt. Lett. **39**, 5383–5386 (2014).
10. M. Schultze, K. Ramasesha, C. D. Pemmaraju, S. A. Sato, D. Whitmore, A. Gandman, J. S. Prell, L. J. Borja, D. Prendergast, K. Yabana, D. M. Neumark, and S. R. Leone, "Attosecond band-gap dynamics in silicon," Science **346**, 1348–1352 (2014).
11. H. Mashiko, K. Oguri, T. Yamaguchi, A. Suda, and H. Gotoh, "Petahertz optical drive with wide-bandgap semiconductor," Nat. Phys. **12**, 741–745 (2016).
12. M. Lucchini, S. A. Sato, A. Ludwig, J. Herrmann, M. Volkov, L. Kasmi, Y. Shinohara, K. Yabana, L. Gallmann, and U. Keller, "Attosecond dynamical Franz-Keldysh effect in polycrystalline diamond," Science **353**, 916–919 (2016).
13. M. Zürch, H. T. Chang, L. J. Borja, P. M. Kraus, S. K. Cushing, A. Gandman, C. J. Kaplan, M. H. Oh, J. S. Prell, D. Prendergast, C. D. Pemmaraju, D. M. Neumark, and S. R. Leone, "Direct and simultaneous observation of ultrafast electron and hole dynamics in germanium," Nat. Commun. **8**, 15734 (2017).
14. D. Popmintchev, B. R. Galloway, M.-C. Chen, F. Dollar, C. A. Mancuso, A. Hankla, L. Miaja-Avila, G. O'Neil, J. M. Shaw, G. Fan, S. Ališauskas, G. Andriukaitis, T. Balčiunas, O. D. Mücke, A. Pugzlys, A. Baltuška, H. C. Kapteyn, T. Popmintchev, and M. M. Murnane, "Near- and extended-edge x-ray-absorption fine-structure spectroscopy using ultrafast coherent high-order harmonic supercontinua," Phys. Rev. Lett. **120**, 93002 (2018).
15. Y. Pertot, C. Schmidt, M. Matthews, A. Chauvet, M. Huppert, V. Svoboda, A. Von Conta, A. Tehlar, D. Baykusheva, J. Wolf, and H. J. Wörner, "Time-resolved x-ray absorption spectroscopy with a water window high-harmonic source," Science **355**, 264–267 (2017).
16. A. R. Attar, A. Bhattacherjee, C. D. Pemmaraju, K. Schnorr, K. D. Closser, D. Prendergast, and S. R. Leone, "Femtosecond x-ray spectroscopy of an electrocyclic ring-opening reaction," Science **356**, 54–59 (2017).
17. S. L. Cousin, F. Silva, S. Teichmann, M. Hemmer, B. Buades, and J. Biegert, "Carbon K-edge NEXFAS spectroscopy from a table-top soft x-ray high harmonics source driven by sub-2-cycle, CEP stable, 1.85-μm 1-kHz laser pulses," Opt. Lett. **39**, 5383–5386 (2014).
18. S. M. Teichmann, F. Silva, S. L. Cousin, M. Hemmer, and J. Biegert, "0.5-keV Soft X-ray attosecond continua," Nat. Commun. **7**, 11493 (2016).
19. S. L. Cousin, N. Di Palo, B. Buades, S. M. Teichmann, M. Reduzzi, M. Devetta, A. Kheifets, G. Sansone, and J. Biegert, "Attosecond streaking in the water window: a new regime of attosecond pulse characterization," Phys. Rev. X **7**, 41030 (2017).
20. A. G. Marinopoulos, L. Reining, A. Rubio, and V. Olevano, "Ab initio study of the optical absorption and wave-vector-dependent dielectric response of graphite," Phys. Rev. B **69**, 245419 (2004).
21. N. Ooi, A. Rairkar, and J. B. Adams, "Density functional study of graphite bulk and surface properties," Carbon **44**, 231–242 (2006).
22. G. te Velde, F. M. Bickelhaupt, E. J. Baerends, C. Fonseca Guerra, S. J. A. van Gisbergen, J. G. Snijders, and T. Ziegler, "Chemistry with ADF," J. Comput. Chem. **22**, 931–967 (2001).
23. C. F. Guerra, J. G. Snijders, G. te Velde, and E. J. Baerends, "Towards an order-N DFT method," Theor. Chem. Acc. **99**, 391–403 (1998).
24. T. N. Vrije, *ADF2017, SCM, Theoretical Chemistry* (Universiteit Amsterdam, 2016).
25. R. A. Rosenberg, P. J. Love, and V. Rehn, "Polarization-dependent C(K) near-edge x-ray-absorption fine structure of graphite," Phys. Rev. B **33**, 4034–4037 (1986).
26. P. A. Brühwiler, A. J. Maxwell, C. Puglia, A. Nilsson, S. Anderson, and N. Martensoon, "pi* and sigma* excitons in C- 1s absorption of graphite," Phys. Rev. Lett. **74**, 614–617 (1995).
27. R. Ahuja, P. Brühwiler, J. Wills, B. Johansson, N. Mårtensson, and O. Eriksson, "Theoretical and experimental study of the graphite 1s x-ray absorption edges," Phys. Rev. B **54**, 14396–14404 (1996).
28. T. Hemraj-Benny, S. Banerjee, S. Sambasivan, M. Balasubramanian, D. A. Fischer, G. Eres, A. A. Puretzky, D. B. Geohegan, D. H. Lowndes, W. Han, J. A. Misewich, and S. S. Wong, "Near-edge X-ray absorption fine structure spectroscopy as a tool for investigating nanomaterials," Small **2**, 26–35 (2006).
29. B. Watts, L. Thomsen, and P. C. Dastoor, "Methods in carbon K-edge NEXAFS: experiment and analysis," J. Electron Spectrosc. Relat. Phenom. **151**, 105–120 (2006).
30. J. A. Brandes, G. D. Cody, D. Rumble, P. Haberstroh, S. Wirick, and Y. Gelinas, "Carbon K-edge XANES spectromicroscopy of natural graphite," Carbon **46**, 1424–1434 (2008).
31. M. Papagno, A. Fraile Rodríguez, Ç. Ö. Girit, J. C. Meyer, A. Zettl, and D. Pacilé, "Polarization-dependent C K near-edge X-ray absorption fine-structure of graphene," Chem. Phys. Lett. **475**, 269–271 (2009).
32. B. J. Schultz, C. J. Patridge, V. Lee, C. Jaye, P. S. Lysaght, C. Smith, J. Barnett, D. A. Fischer, D. Prendergast, and S. Banerjee, "Imaging local electronic corrugations and doped regions in graphene," Nat. Commun. **2**, 372 (2011).

33. B. Ravel and M. Newville, "ATHENA, ARTEMIS, HEPHAESTUS: data analysis for X-ray absorption spectroscopy using IFEFFIT," J. Synchrotron Rad. **12**, 537–541 (2005).

34. J. J. Rehr, J. J. Kas, F. D. Vila, M. P. Prange, and K. Jorissen, "Parameter-free calculations of X-ray spectra with FEFF9," Phys. Chem. Chem. Phys. **12**, 5503–5513 (2010).

35. G. Comelli, J. Stöhr, W. Jark, and B. B. Pate, "Extended x-ray-absorption fine-structure studies of diamond and graphite," Phys. Rev. B **37**, 4383–4389 (1988).

36. T. Tanaka, N. Matsubayashi, M. Imamura, and H. Shimada, "Synchronous scanning of undulator gap and monochromator for XAFS measurements in soft x-ray region," J. Synchrotron Radiat. **8**, 345–347 (2001).